iScience

CellPress
OPEN ACCESS

Article

# Stearic acid alleviates aortic medial degeneration through maintaining mitochondrial dynamics homeostasis via inhibiting JNK/MAPK signaling

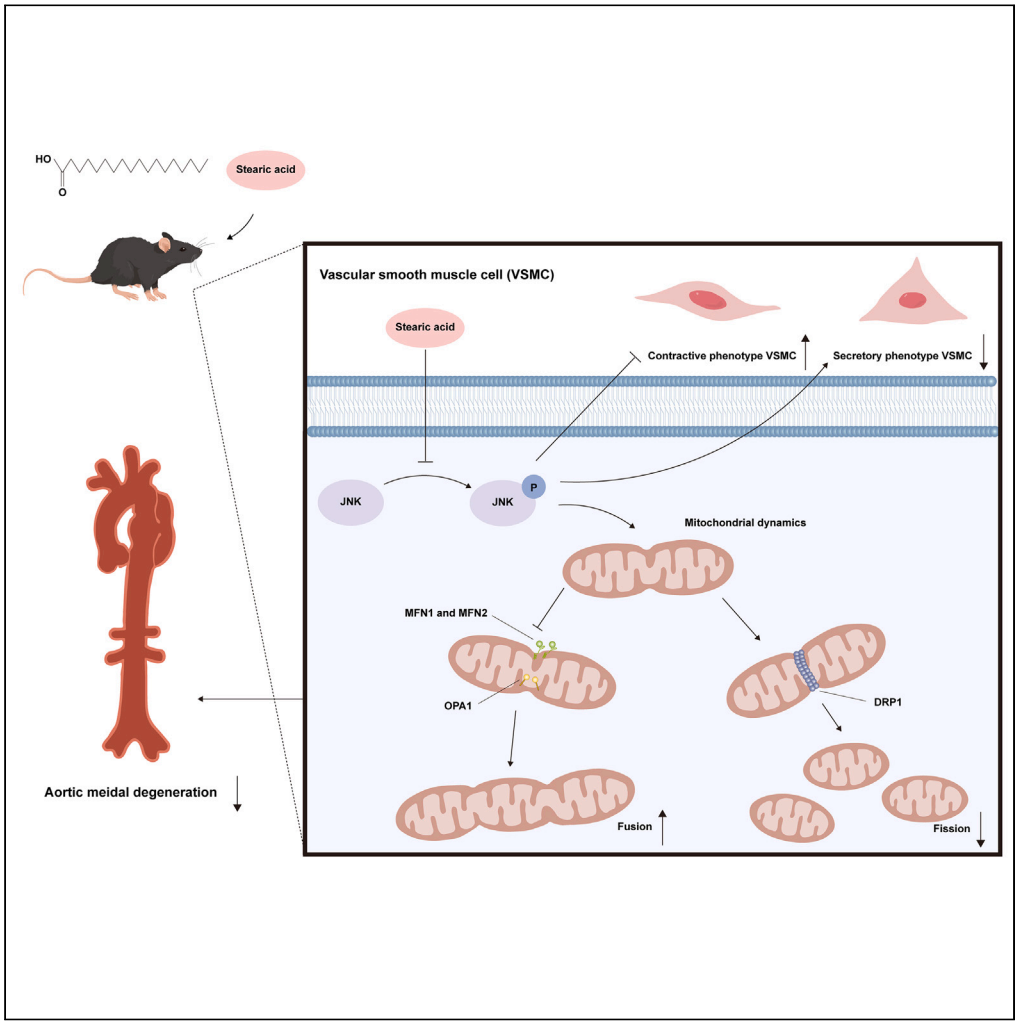


Kexin Wang, Xiaoping Xie, Xiaoping Hu, Zhiwei Wang, Jun Xia, Qi Wu

xiaoping8205@whu.edu.cn

## Highlights

Stearic acid alleviates aortic dissection both *in vivo* and in *vitro*

Stearic acid maintains mitochondrial dynamics homeostasis

Stearic acid inhibits JNK/MAPK signaling, playing a protective role in aortic dissection

Wang et al., iScience 27, 110594
September 20, 2024 
https://doi.org/10.1016/j.isci.2024.110594

iScience

CellPress
OPEN ACCESS

Article

# Stearic acid alleviates aortic medial degeneration through maintaining mitochondrial dynamics homeostasis via inhibiting JNK/MAPK signaling

Kexin Wang,[1,2,3,4,5] Xiaoping Xie,[1,2,3,4,5] Xiaoping Hu,[1,2,3,4,6,*] Zhiwei Wang,[1,2,3,4] Jun Xia,[1,2] and Qi Wu[1,2]

## SUMMARY

**Aortic dissection is characterized pathologically by aortic medial degeneration (AMD) where disturbance of mitochondrial dynamics may be involved. Stearic acid (SA) can promote mitochondrial fusion and improve mitochondrial function. Here, we established an AMD mouse model through oral administration of β-aminopropionitrile (BAPN) and a cellular model by treating primary vascular smooth muscle cells (VSMCs) with Angiotensin-II to explore the potential role of SA in AMD. Our results showed SA reduced AMD and prolonged survival of BAPN-treated mice. Excessive mitochondrial fission was observed during AMD both *in vivo* and *in vitro*, and SA reduced mitochondrial fission and increased fusion. Additionally, SA promoted expression of contractile phenotype markers of VSMCs. At the molecular level, SA reduced AMD by inhibiting JNK/MAPK signaling. Our study suggests SA can promote mitochondrial fusion and increase the contractile phenotype of VSMCs by inhibiting JNK/MAPK signaling, thereby reducing AMD formation and possibly the consequent risk of aortic dissection.**

## INTRODUCTION

Aortic dissection (AD) can be a management challenge, as its onset is often insidious, making an early diagnosis difficult. AD, especially type A aortic dissection (TAAD), carries an extremely high mortality rate if not immediately surgically repaired.[1] Although surgical intervention can increase survival rates for TAAD significantly, the operative mortality remains high. In-hospital mortality over the past decade has been reported to be 22%.[2,3] Risk factors for AD include hypertension, dyslipidemia, advanced age, and genetic disorders such as Loeys–Dietz syndrome and Marfan syndrome.[4] The main pathological feature of AD is aortic medial degeneration (AMD), which is associated with increased proliferation, migration, apoptosis, and abnormal phenotype of vascular smooth muscle cells (VSMCs) together with weakening of the extracellular matrix and vascular inflammation.[5–7] However, the specific mechanisms underlying AMD pathogenesis are still poorly understood, mandating further study of the pathobiology of AMD to elucidate potential therapeutic targets and treatment approaches.

Stearic acid (C18:0, SA) is a type of saturated fatty acid (SFA) abundant in many Western diets.[8] Without SA, *Drosophila* die as early larvae,[9] suggesting that SA plays an important physiological role. For example, previous studies have reported that SA may have antifibrotic properties by regulating profibrotic signaling, playing a protective role in idiopathic pulmonary fibrosis.[10] Additionally, SA can protect cortical neurons from oxidative stress by boosting antioxidant enzymes, serving a neuroprotective function.[11] Recently, the role of SA in the cardiovascular system has also drawn considerable attention. Compared with other SFAs like palmitic acid (PA), dietary SA does not increase the risk of developing atherosclerosis, a risk factor for AMD.[12] If anything, SA tends to lower low-density lipoprotein (LDL) cholesterol levels,[13–15] protecting against atherosclerosis, and higher circulating SA concentrations are associated with decreased blood pressure, enhanced cardiac function, and a reduced risk of cancer.[16,17] Moreover, dietary SA (but not PA) increases fatty acid beta-oxidation *in vivo* in humans, indicating that SA reduces fat accumulation.[18]

Mitochondrial dynamics refer to a constant processes of mitochondrial fission and fusion, which provide energy for the cell and regulate autophagy, calcium homeostasis, signal transduction, and apoptosis.[19] The mitochondrion is enveloped by an inner and an outer membrane.[20] Proteins distributed on these membranes regulate mitochondrial fission and fusion.[21] Specifically, mitofusin 1 (MFN1) and mitofusin 2 (MFN2) are associated with the mitochondrial outer membrane fusion, while optic atrophy protein 1 (OPA1) is related to the inner membrane fusion.[22] In mammals, mitochondrial fission is coordinated by dynamin-related protein 1 (DRP1), with mitochondrial fission 1 protein (FIS1) and

[1]Department of Cardiovascular Surgery, Renmin Hospital of Wuhan University, 238 Jiefang Road, Wuhan 430060, Hubei Province, P.R. China
[2]Central Laboratory, Renmin Hospital of Wuhan University, 9 Zhangzhidong Road, Wuhan 430060, Hubei Province, P.R. China
[3]Hubei Key Laboratory of Cardiology, 238 Jiefang Road, Wuhan 430060, Hubei Province, P.R. China
[4]Cardiovascular Research Institute, Wuhan University, 238 Jiefang Road, Wuhan 430060, Hubei Province, P.R. China
[5]These authors contributed equally
[6]Lead contact
*Correspondence: xiaoping8205@whu.edu.cn
https://doi.org/10.1016/j.isci.2024.110594

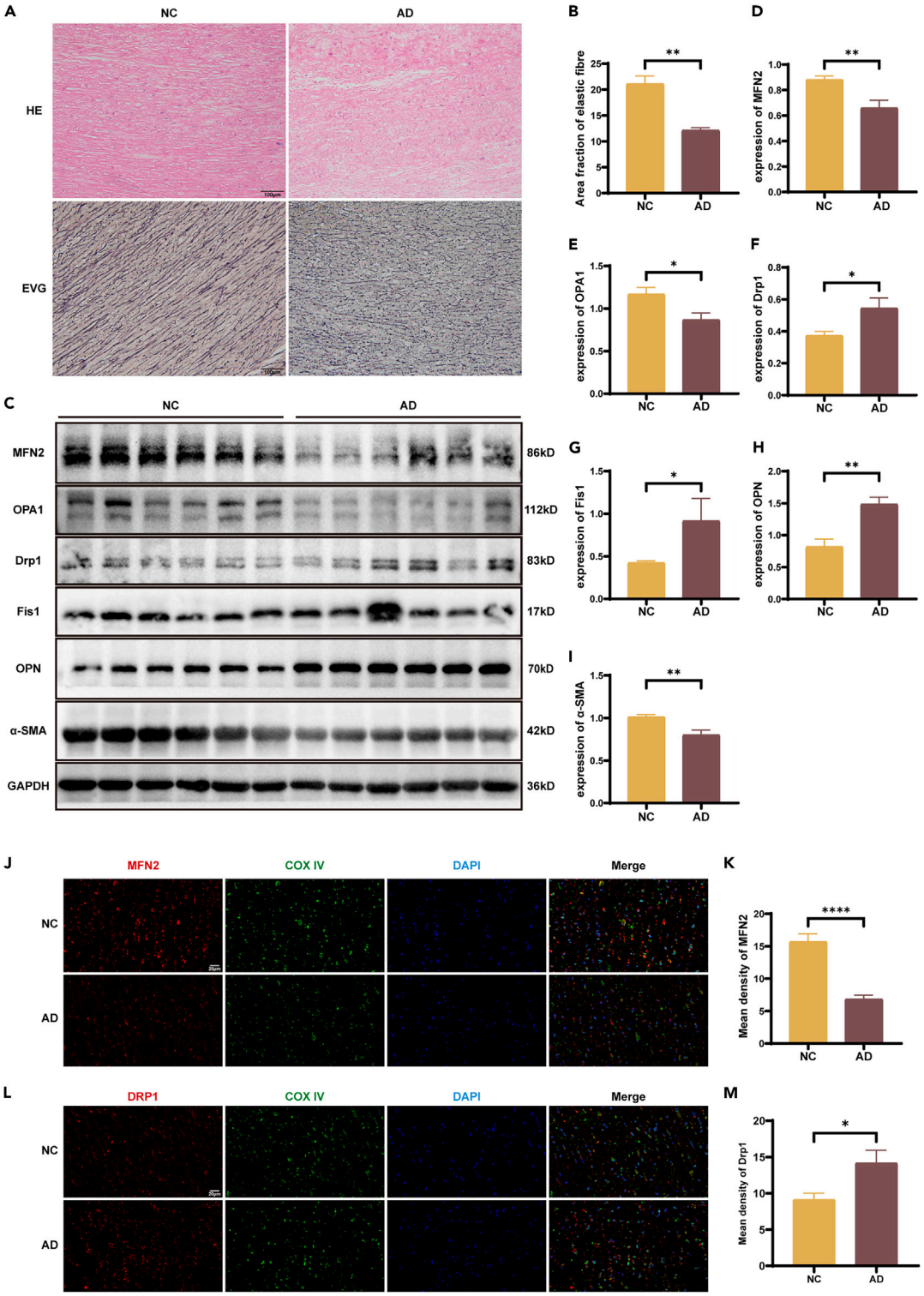


**Figure 1. Imbalance of mitochondrial dynamics and phenotype switching of VSCMs in AD patients**

(A) Representative images of H&E– and EVG-stained sections of the aortic media.

(B) Quantification of the percentage area of elastic fibers ($n$ = 4).

(C–I) Representative western blots of MFN2, OPA1, DRP1, FIS1, OPN and α-SMA in the aortic media of AD patients and organ donors, along with their respective quantifications ($n$ = 6).

(J–M) Co-localization of COX IV and MFN2, COX IV and DRP1, and quantifications of immunofluorescence for MFN2 and DRP1 ($n$ = 6). Data are derived from three independent experiments, and all data are presented as mean ± S.E.M. *$p < 0.05$, **$p < 0.01$, ****$p < 0.0001$.

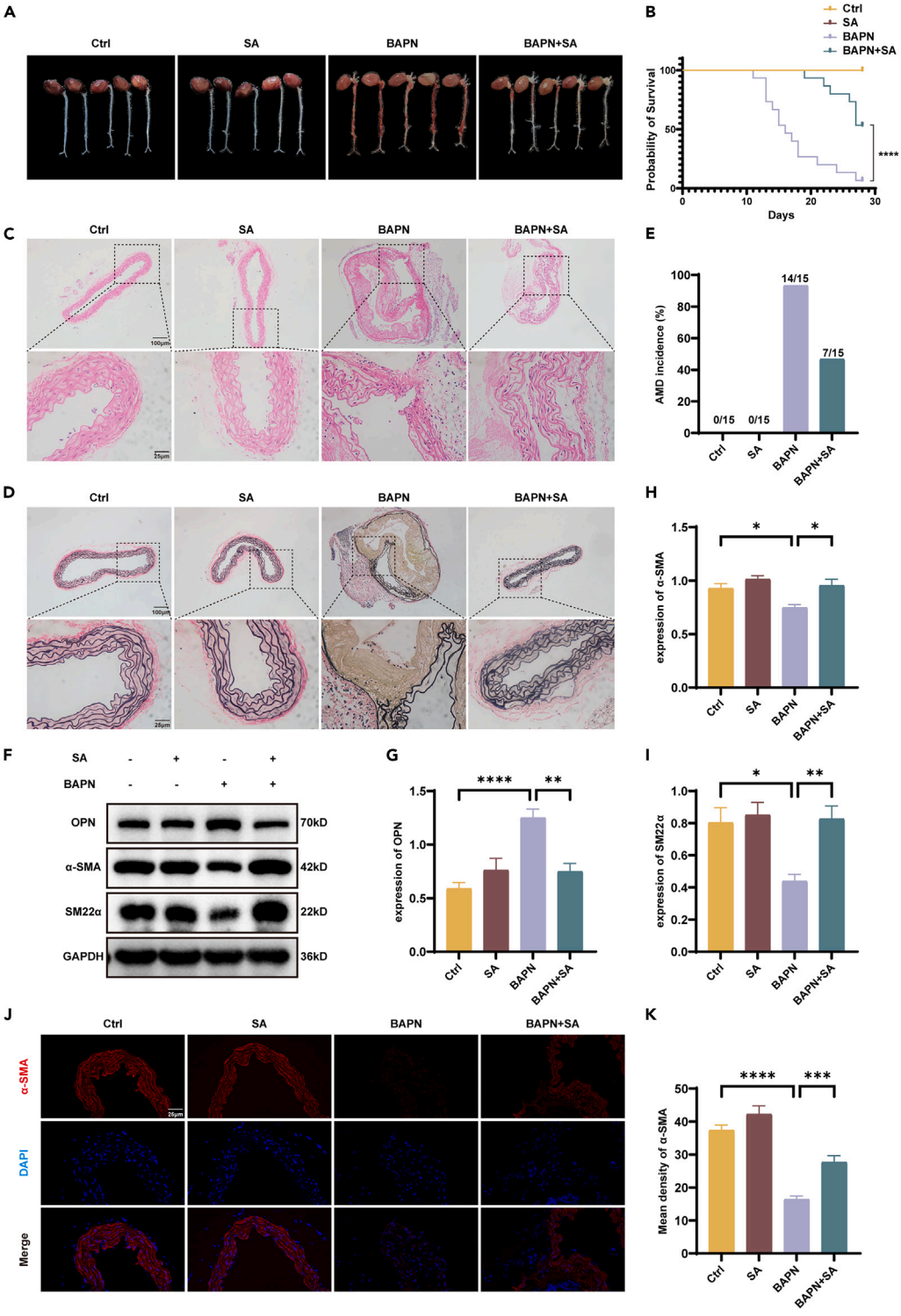


**Figure 2. SA reduced the formation of BAPN-induced AMD in mice**

(A) Representative images of mouse aortic specimens.

(B) Survival curves.

(C and D) Representative images of H&E– and EVG-stained sections of the aortas from these four groups.

(E) AMD incidence of C57BL/6J mice of each group.

(F–I) Representative western blots of OPN, α-SMA and SM22α, along with statistical analyses of their expression levels.

(J and K) Representative images and quantification of α-SMA immunofluorescence in mouse aortas. Data are derived from three independent experiments, and all data are presented as mean ± S.E.M. *$p < 0.05$, **$p < 0.01$, ***$p < 0.001$, ****$p < 0.0001$.

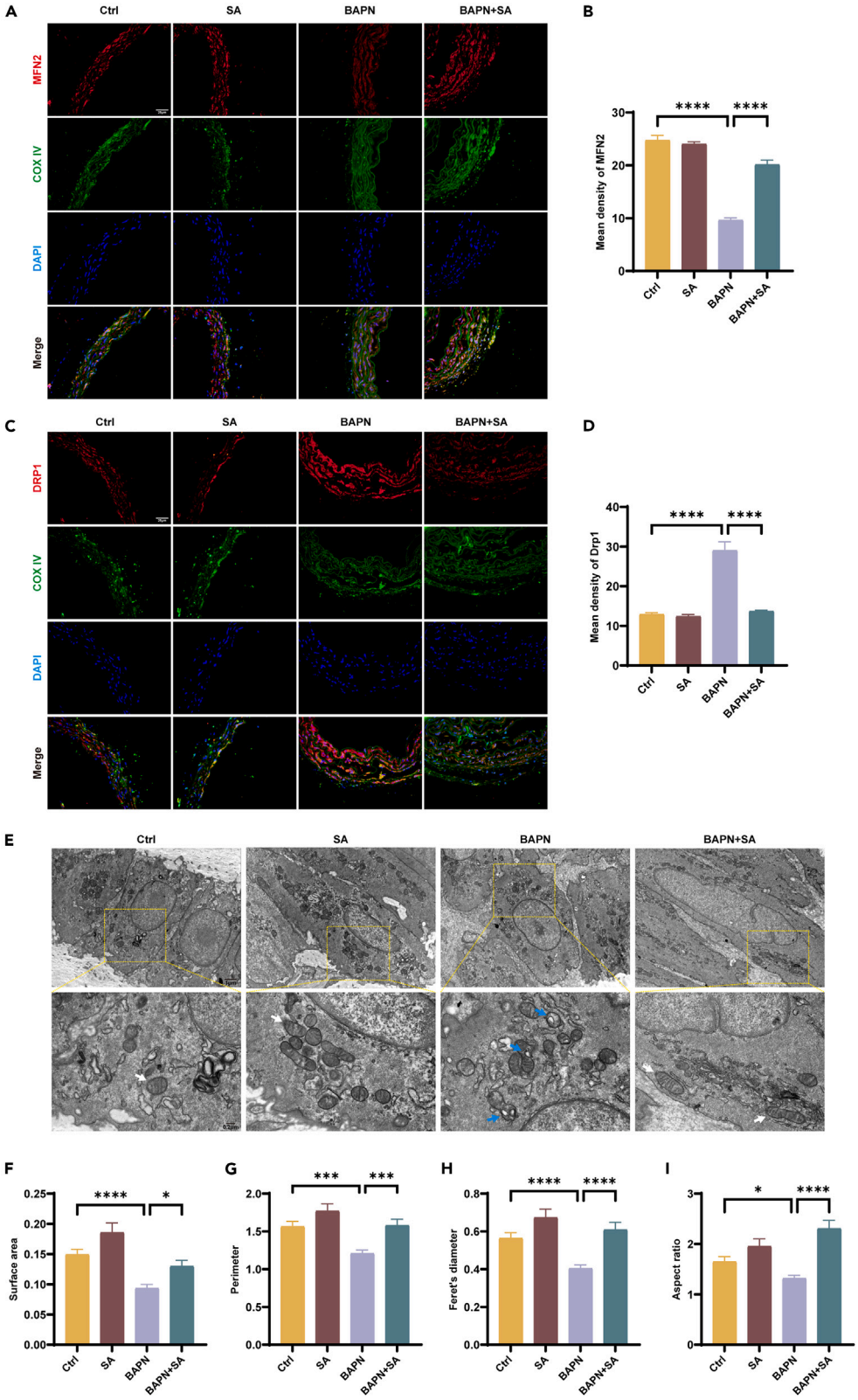
A
Ctrl
SA
BAPN
BAPN+SA
MFN2
COX IV
DAPI
Merge
B
Mean density of MFN2
****
****
C
DRP1
D
Mean density of Drp1
E
F
Surface area
****
*
G
Perimeter
***
***
H
Feret's diameter
****
****
I
Aspect ratio
*
****

**Figure 3. SA promotes mitochondrial fusion in VSMCs of AMD mice**

(A–D) Representative Co-localization images of MFN2 and COX IV, DRP1 and COX IV in mouse aortic tissues, along with quantification of average fluorescence intensity.

(E) Representative TEM images of VSMCs in the aortas of the four mouse groups. White arrows indicate normal mitochondria, while blue arrows represent mitochondria with abnormal structures.

(F–I) Quantification of mitochondrial morphological metrics such as mitochondrial surface area, perimeter, Feret's diameter, and aspect ratio. >30 mitochondria were measured in each group. Data are derived from three independent experiments, and all data are presented as mean ± S.E.M. *$p < 0.05$, ***$p < 0.001$, ****$p < 0.0001$.

others recruiting DRP1 to the outer membrane to exert its function.[23] The relative balance between fission and fusion is critical for preserving the mitochondrial quality and function, therefore, ensuring normal cellular activities. Disturbance of mitochondrial dynamics is tied to neurodegenerative diseases, cardiovascular diseases, cancer, and diabetes,[24–27] and recent investigations have shown that excessive mitochondrial fission may be vital to exacerbating AMD.[28,29] Despite this, the specific mechanisms by which an imbalance in mitochondrial fusion and fission affects AMD remain incompletely understood and warrant further investigation.

SA has been shown to regulate mitochondrial morphology and function.[9] Dietary SA might rescue the mitochondrial dysfunction in *Drosophila* caused by genetic defects such as loss of *Pink* or *Parkin*.[9] Interestingly, dietary SA induced mitochondrial fusion within a few hours of eating.[18] Furthermore, SA can promote mitochondrial fusion by stearoylating the transferrin receptor (TFR1).[9] Intriguingly, our previous study detected increased expression of TFR1 in aortic media during the onset of AD,[30] suggesting that SA may play a role in AMD.

Given this critical role for SA in regulating mitochondrial function and lipid metabolism, we hypothesized that SA may protect against AMD. To test this, we established a mouse model of AMD through oral administration of β-aminopropionitrile (BAPN) to investigate the effect and mechanisms of SA in AMD.

## RESULTS

### Mitochondrial fusion is significantly decreased and phenotypic switching of VSMCs from contractile to synthetic is increased in the aortic tissue of patients with AMD

Aortic specimens were obtained from patients with AD and organ donors and subjected to H&E and EVG staining. Examination of H&E-stained sections revealed a reduced number of cells and disorganized extracellular matrix in the aortic media of AD patients (Figure 1A). Furthermore, EVG staining showed a disordered arrangement of significantly fewer elastic fibers in the aortas of AD patients (Figures 1A and 1B).

Proteins were extracted from the tissue specimens for western blot analysis. The expression of proteins related to mitochondrial fusion, such as MFN2 and OPA1, were downregulated, and proteins associated with mitochondrial fission, including DRP1 and FIS1, were upregulated (Figures 1C–1G), suggesting reduced mitochondrial fusion and excessive fission in the aortic tissues of AD patients. Subsequently, we performed immunofluorescence analysis and similarly observed that, in AD patients, aortic media expression of MFN2 (Figures 1J and 1K) and OPA1 (Figures S1A and S1B) was significantly lower than in the normal control (NC) group ($p < 0.0001$ and $p < 0.001$, respectively), while expression of DRP1 was significantly upregulated in the aortic media from AD patients ($p < 0.05$) (Figures 1L and 1M). The immunofluorescence analysis supported our conclusion that, during AD progression, mitochondrial fusion decreases and mitochondrial fission increases in the aortic media. More importantly, we performed dual immunofluorescence staining for COX IV with MFN2 and COX IV with DRP1, thereby confirming the expression of these mitochondrial dynamics-related proteins within the mitochondria. Additionally, we investigated the phenotype transformation of VSMCs in human aortic tissues. WB results indicated that, compared to the NC group, the expression of the contractile phenotype marker α-SMA was decreased, while the expression of the synthetic phenotype marker OPN was increased in the AD group (Figures 1C–1I). This suggests an enhanced transformation of VSMCs from a contractile to a synthetic phenotype in the aortic tissues of AD patients.

### Stearic acid attenuates AMD formation induced by BAPN *in vivo*

To investigate the potential effects of SA on AD, mice were fed a 17% SA diet or a regular diet for 5 days in advance of model initiation with BAPN for 28 days. After 28 days, the mortality rate of the BAPN group was 93.3% (14 of 15), while the mortality rate of the BAPN+SA group was 46.7% (7 of 15) (Figure 2B). Mice in the Ctrl and SA groups did not develop AMD or die (Figures 2A and 2B). Moreover, survival of mice in the BAPN+SA group was significantly longer than those in the BAPN group ($p$ <0.0001) (Figure 2B).

All specimens were harvested at 28 days or upon death (Figure 2A). Examination of H&E-stained sections revealed varying degrees of false lumens and rupture in both the BAPN and BAPN+SA groups (Figure 2C). EVG staining showed that elastin fiber damage in the aorta media was greater in the BAPN group than the BAPN+SA group (Figure 2D). Therefore, we concluded that SA reduced the formation and severity of AMD, consequently decreasing the mortality rate in mice with AD.

### Stearic acid promotes mitochondrial fusion and regulates the phenotype switching in BAPN-treated mice

To assess levels of mitochondrial fusion and fission *in vivo*, we applied immunofluorescence to detect proteins associated with mitochondrial dynamics to tissue sections. Compared with the control group, there was significantly increased expression of Drp1 in the aortic tissue of the BAPN group (Figures 3C and 3D), while expression of MFN2 markedly decreased (Figures 3A and 3B), consistent with the findings observed in

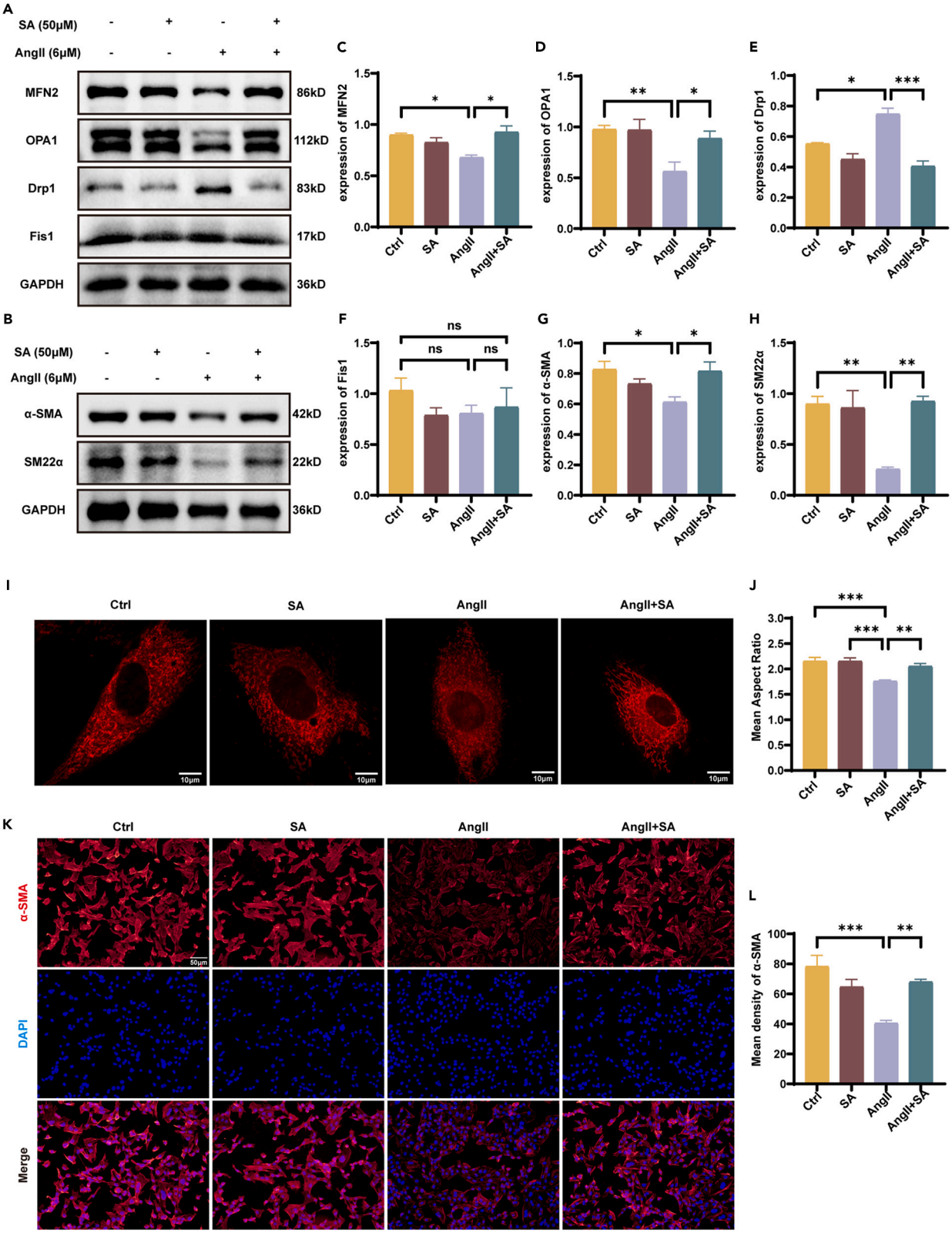
A
SA (50μM)
AngII (6μM)
MFN2
OPA1
Drp1
Fis1
GAPDH
86kD
112kD
83kD
17kD
36kD
B
SA (50μM)
AngII (6μM)
α-SMA
SM22α
GAPDH
42kD
22kD
36kD
C
expression of MFN2
D
expression of OPA1
E
expression of Drp1
F
expression of Fis1
G
expression of α-SMA
H
expression of SM22α
Ctrl
SA
AngII
AngII+SA
ns
I
Ctrl
SA
AngII
AngII+SA
10μm
J
Mean Aspect Ratio
K
α-SMA
DAPI
Merge
50μm
L
Mean density of α-SMA

**Figure 4. SA regulates mitochondrial fusion and phenotypic switching in VSMCs *in vitro***

(A–H) Representative western blots of mitochondrial dynamics-related proteins MFN2, OPA1, DRP1, and FIS1 and markers of phenotypic switching α-SMA and SM22α, along with statistical analyses of their expression levels.

(I and J) Representative images of VSMC mitochondria stained with MitoTracker and captured by confocal microscopy, along with quantification of the aspect ratio of mitochondria.

(K and L) Representative images of α-SMA immunofluorescence in VSMCs and quantification of average fluorescence intensity. Data are derived from three independent experiments, and all data are presented as mean ± S.E.M. *$p < 0.05$, **$p < 0.01$, ***$p < 0.001$. ns = no significant difference.

human specimens. However, this effect was blunted by SA, resulting in reduced mitochondrial fission and increased fusion (Figures 3A–3D). Furthermore, we performed dual immunofluorescence staining of these proteins with COX IV, and the results indicated that MFN2 and DRP1 are localized within the mitochondria (Figures 3A and 3C).

Subsequently, we employed TEM to directly observe mitochondrial structures and quantified mitochondrial morphology using the metrics of surface area, perimeter, Feret's diameter, and aspect ratio, as previously.[31] In the BAPN group, abnormal mitochondria were observed, including the disappearance of mitochondrial cristae and the presence of intramitochondrial vacuoles. In contrast, fewer abnormal mitochondria were noted in the BAPN+SA group (Figure 3E). In quantitative analyses, mitochondria in the BAPN group had a smaller surface area, perimeter, Feret's diameter, and aspect ratio than those in the control group, indicating an increase in fragmented mitochondria (Figures 3F–3I). However, SA reversed this phenotype, consistent with protein expression.

Furthermore, AMD is commonly marked by phenotype switching of VSMCs, leading to decreased expression of proteins associated with VSMC contraction and increased expression of proteins linked to synthetic VSMCs, including α-SMA, SM22α and OPN.[25,32] Western blot analysis revealed that SA upregulated the expression of α-SMA, SM22α and downregulated the expression of OPN in mice with BAPN-induced AMD, leading to a decrease in the switching of VSMCs from a contractile to a synthetic phenotype (Figures 2F–2I). Furthermore, consistent results were obtained from immunofluorescence staining of α-SMA in mouse aortic tissues (Figures 2J and 2K).

## Stearic acid promotes mitochondrial fusion and regulates phenotype switching in AngII-induced VSMCs

We next evaluated mitochondrial dynamics *in vitro*. There were no significant differences in mitochondrial fission or fusion protein expression between control and SA groups. However, compared with controls, AngII treatment significantly increased expression of DRP1 in VSMCs (Figures 4A and 4E), while the expressions of MFN2, OPA1 (Figures 4A–4D), and MFN1 (Figures S2A and S2B) were significantly lower than in control cells. Moreover, expression of MFN2, OPA1 (Figures 4A–4D), and MFN1 (Figures S2A and S2B) was higher in the SA + AngII group than in the AngII group, while expression of DRP1 was lower than in the AngII group (Figures 4A and 4E). However, FIS1 expression was not significantly different between groups (Figures 4A and 4F).

Consistent with the western blotting results, MitoTracker staining for mitochondria revealed that VSMCs treated with AngII exhibited fragmented mitochondria with a lower aspect ratio, indicating increased mitochondrial fission and reduced fusion (Figures 4I and 4J). As expected, SA mitigated the effect of AngII. Furthermore, we examined expression of α-SMA and SM22α, markers of the contractile phenotype of VSMCs, to determine phenotypic switching. In VSMCs treated with AngII, expression of α-SMA and SM22α was significantly downregulated (Figures 4B–4H) compared to controls. By contrast, in VSMCs co-treated with AngII and SA, the expression of α-SMA and SM22α was increased compared with cells treated solely with AngII. Immunofluorescence analysis was consistent with the western blot results (Figures 4K and 4L). Taken together, SA enhances the mitochondrial fusion and contractile phenotype of VSMCs in AngII-induced AD.

## Stearic acid promotes mitochondrial fusion and a contractile phenotype in AngII-induced VSMCs through JNK/MAPK signaling

To investigate the potential mechanisms by which SA affects the formation of AD, we noted that the c-Jun N-terminal kinase/mitogen-activated protein kinase (JNK/MAPK) pathway plays a crucial role in regulating cell growth, differentiation, and apoptosis,[33] all of which are significantly associated with the development of AD.[32,34] Therefore, JNK and phosphorylated JNK (*p*-JNK) were quantified to measure activation of the JNK/MAPK signaling pathway.

First, in human specimens, western blotting results indicated an increase in JNK activation in AD patients, with a significantly higher *p*-JNK/JNK ratio compared with organ donors (Figures 5A and 5B). Furthermore, consistent with the western blotting results, immunohistochemical analysis of human specimens revealed a marked increase in the average optical density of *p*-JNK in AD patients (Figures 5C and 5D).

*p*-JNK/JNK levels were higher during AMD both *in vitro* and *in vivo*, and SA rescued this effect (Figures 5E–5J), consistent with our findings in human specimens. To investigate whether SA exerts its effects through the JNK/MAPK signaling pathway *in vitro*, we introduced a JNK-specific agonist, anisomycin (ANI), to VSMCs divided into four groups: Ctrl, AngII, AngII+SA, and AngII+SA+ANI. Western blot analysis revealed that *p*-JNK/JNK levels in VSMCs significantly increased after treatment with ANI compared with the AngII+SA group (Figures 6B and 6I). This was corroborated by immunofluorescence analysis (Figures 6N and 6O). Moreover, expression of MFN2, OPA1 (Figures 6A–6D), and MFN1 (Figures S3A and S3B) was significantly lower in the AngII+SA+ANI group than in the AngII+SA group, with upregulated expression of DRP1, while FIS1 expression was not significantly different between groups (Figures 6A–6F), indicating that ANI reversed the SA-promoted mitochondrial fusion in VSMCs.

Similarly, mitochondrial staining with MitoTracker showed an increase in fragmented mitochondria and a decrease in aspect ratio in VSMCs in the AngII+SA+ANI group compared with the AngII+SA group (Figures 6J and 6K), consistent with the western blotting results.

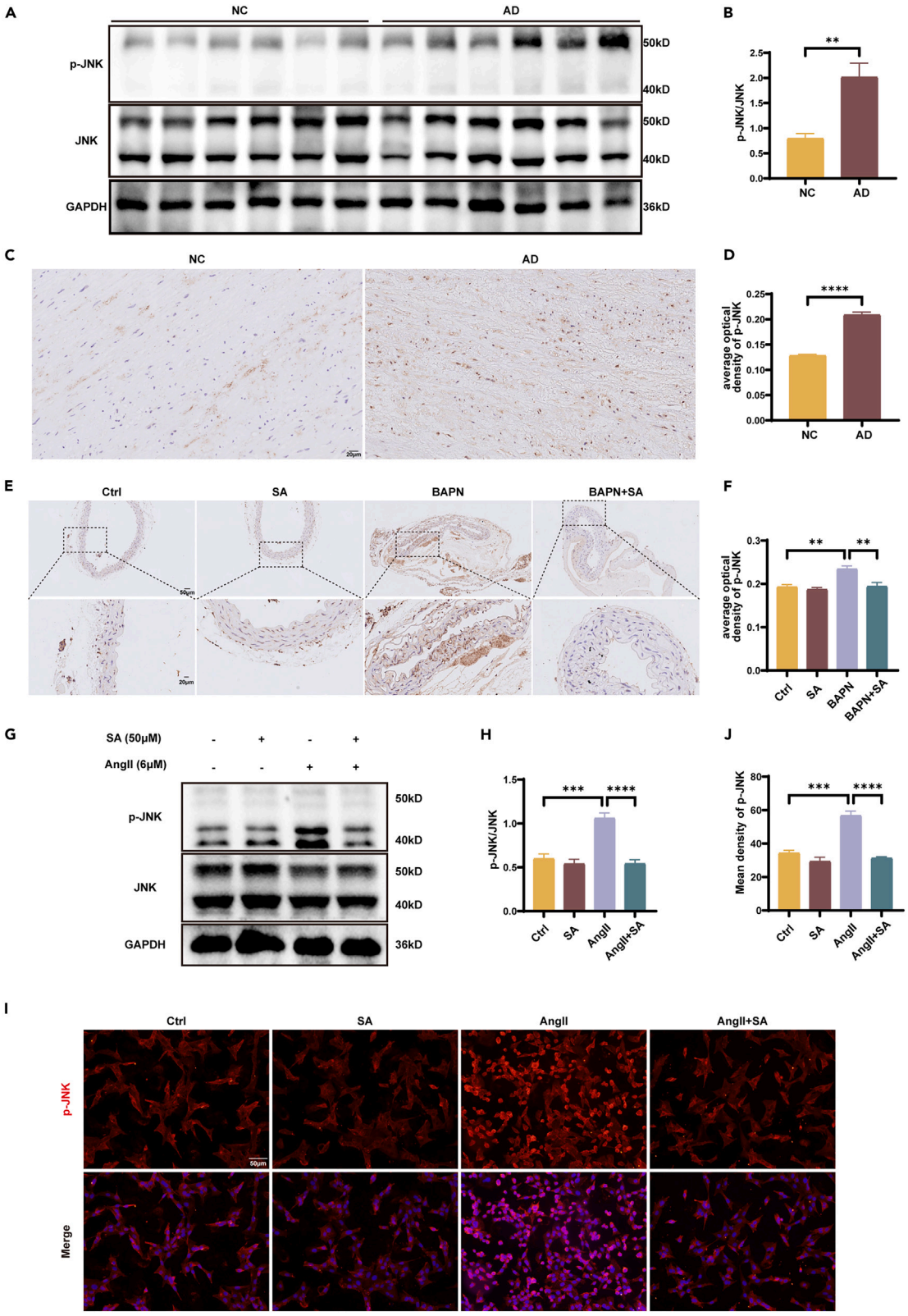
A
NC
AD
p-JNK
JNK
GAPDH
50kD
40kD
50kD
40kD
36kD
B
p-JNK/JNK
**
NC
AD
C
NC
AD
D
average optical density of p-JNK
****
NC
AD
E
Ctrl
SA
BAPN
BAPN+SA
F
average optical density of p-JNK
**
**
Ctrl
SA
BAPN
BAPN+SA
G
SA (50μM)
AngII (6μM)
p-JNK
JNK
GAPDH
50kD
40kD
50kD
40kD
36kD
H
p-JNK/JNK
***
****
Ctrl
SA
AngII
AngII+SA
J
Mean density of p-JNK
***
****
Ctrl
SA
AngII
AngII+SA
I
Ctrl
SA
AngII
AngII+SA
p-JNK
Merge

**Figure 5. SA inhibits phosphorylation of JNK both *in vivo* and *in vitro***

(A and B) Representative western blots of phosphorylated JNK (*p*-JNK) and total JNK in the aortic media of AD patients and organ donors, along with calculation of the *p*-JNK/JNK ratio.

(C and D) Representative immunohistochemistry images of *p*-JNK in human aortic media and quantification of the average optical density of *p*-JNK.

(E and F) Representative immunohistochemistry images showing inhibition of JNK phosphorylation by SA in the AMD mouse model, and quantification of the average optical density of *p*-JNK.

(G and H) Representative western blots showing inhibition of JNK activation by SA in AngII-treated VSMCs *in vitro*, along with quantification of the *p*-JNK/JNK ratio.

(I and J) Immunofluorescence images of *p*-JNK in VSMCs and analysis of average fluorescence intensity. Data are derived from three independent experiments, and all data are presented as mean ± S.E.M. $^{**}p < 0.01$, $^{***}p < 0.001$, $^{****}p < 0.0001$.

These findings suggest that SA may promote mitochondrial fusion in VSMCs by inhibiting the activation of JNK/MAPK signaling. Additionally, the SA-induced upregulation of contractile phenotype markers α-SMA and SM22α was reversed upon adding ANI (Figures 6B–6H). Immunofluorescence analysis of VSMCs also revealed that the average fluorescence intensity of α-SMA in the AngII+SA group was significantly higher than in the AngII group, while it was significantly lower in the AngII+SA+ANI group compared with the AngII+SA group (Figure 6L and 6M), suggesting that SA's promotion of the contractile phenotype in VSMCs may be achieved by inhibiting the JNK/MAPK pathway.

### Stearic acid attenuates BAPN-induced AD formation by suppressing activation of JNK/MAPK signaling

We next validated these potential mechanisms in the mouse model. Twenty-four three-week-old male C57BL/6J mice of the similar weight were randomly divided into three groups ($n = 8$ per group): regular diet (Ctrl), BAPN+SA diet (BAPN+SA), and BAPN+SA diet with intraperitoneal injection of ANI (BAPN+SA+ANI) at 10 mg/kg d based on previous research.[35] Ctrl and BAPN+SA groups received daily intraperitoneal injections of saline. Surprisingly, the mortality rate in the BAPN+SA+ANI group was 87.5% (7 out of 8) compared with 50% (4 out of 8) in the BAPN+SA group (Figures 7B and 7E). It was demonstrated in H&E and EVG staining that aortic lesions in BAPN+SA+ANI group were more severe than those in BAPN+SA group (Figures 7C and 7D). Additionally, survival of mice in the BAPN+SA group was significantly longer than those in the BAPN+SA+ANI group (Figure 7B). This suggests that SA's reduction in AD formation may be achieved by inhibiting JNK/MAPK signaling.

### Stearic acid promotes mitochondrial fusion and regulates the phenotype transition in BAPN-treated mice by suppressing JNK/MAPK signaling

To determine whether SA influences mitochondrial dynamics and VSMC phenotypic switching in AMD mice induced by BAPN via the JNK/MAPK signaling pathway, we performed immunofluorescence and immunohistochemistry analyses on murine aortic sections. First, immunohistochemistry results indicated that mice injected intraperitoneally with the JNK-specific agonist ANI exhibited significantly higher expression of *p*-JNK in the aorta compared with the control and BAPN+SA groups (Figures 8A and 8B). Western blot analysis showed that α-SMA, and SM22α expression was significantly lower but expression of OPN increased in the BAPN+SA+ANI group compared with the BAPN+SA group (Figures 7F–7I), indicating a reduction in contractile VSMCs and an increase in synthetic VSMCs. And the results from our immunofluorescence staining of α-SMA were consistent with those observed in the western blot (Figures 7J and 7K). Similarly, compared with mice in the BAPN+SA group, mice injected with ANI showed decreased expression of MFN2 (Figures 8C and 8D) and upregulated expression of DRP1 (Figures 8E and 8F) in the aorta, suggesting that the effects of SA on mitochondrial dynamics were negated by ANI. Similarly, we performed dual immunofluorescence staining for MFN2, DRP1, and the mitochondrial marker protein COX IV respectively. We observed co-localization of these proteins, indicating the distribution of MFN2 and DRP1 within the mitochondria (Figures 8C and 8E). Through direct visualization with TEM, mitochondria in the aorta of mice treated with ANI were swollen and vacuolated (Figure 8G). Finally, we also quantified mitochondrial morphology and found that the mitochondrial perimeter, Feret's diameter, and aspect ratio in VSMCs of the aorta in the ANI treatment group were significantly lower than those in the control and BAPN+SA groups, while the surface area was not significantly different (Figures 8H–8K). These results indicated an increase in fragmented mitochondria, consistent with our immunofluorescence results.

## DISCUSSION

Here we provide the first evidence that SA attenuates the development of AMD induced by BAPN in mice. Furthermore, we elucidated the potential mechanism by which SA influences AMD, namely by inhibiting the JNK phosphorylation, thereby reducing activation of JNK/MAPK signaling. This mechanism promotes mitochondrial fusion in VSMCs and their contractile phenotype, thereby contributing to the suppression of AMD development.

AD and aortic aneurysm are common aortic diseases encountered in cardiovascular surgery, and both share a common pathological basis called AMD.[30] The precise pathogenic mechanisms underlying AMD remain unclear, although hyperlipidemia is a significant risk factor.[36] Patients with AMD often have lipid metabolism disorders, such as increased levels of triglycerides, total cholesterol (TC), and LDL-C and decreased levels of HDL-C and ApoA1.[37] SA appears to influence plasma lipid components, such as reducing LDL-C and TC,[38,39] probably due to the unique physical properties of SA. Fats rich in SA, like lard, have a higher solid fat content at body temperature,

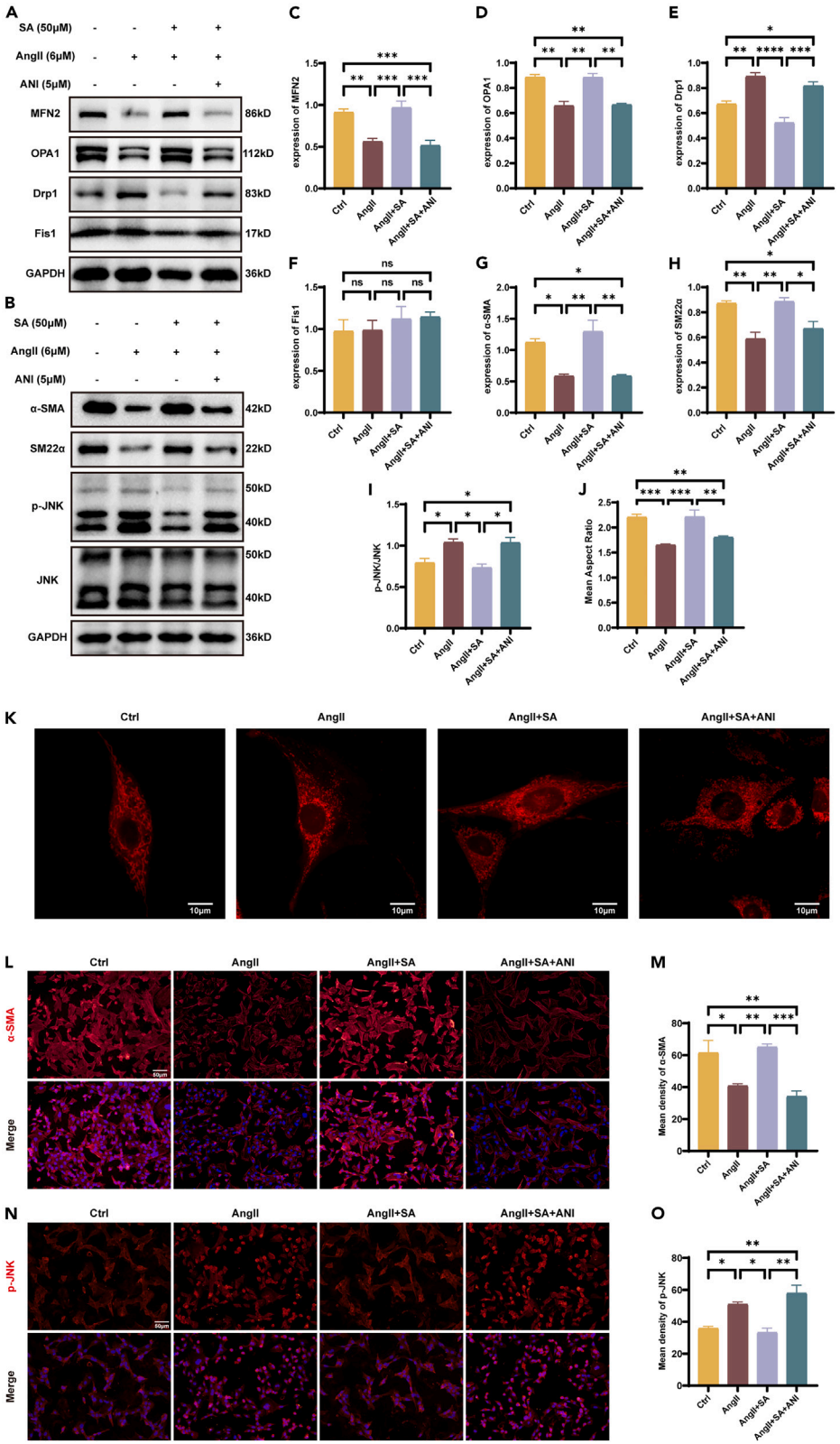
A
SA (50μM)
AngII (6μM)
ANI (5μM)
MFN2
OPA1
Drp1
Fis1
GAPDH
86kD
112kD
83kD
17kD
36kD
B
α-SMA
SM22α
p-JNK
JNK
42kD
22kD
50kD
40kD
C
expression of MFN2
D
expression of OPA1
E
expression of Drp1
F
expression of Fis1
G
expression of α-SMA
H
expression of SM22α
I
p-JNK/JNK
J
Mean Aspect Ratio
Ctrl
AngII
AngII+SA
AngII+SA+ANI
K
10μm
L
α-SMA
Merge
M
Mean density of α-SMA
N
p-JNK
O
Mean density of p-JNK

**Figure 6. Activation of JNK reverses the effects of SA on mitochondrial fusion and AMD formation *in vitro***

(A–I) Representative western blots of MFN2, OPA1, DRP1, FIS1, α-SMA, SM22α as well as typical bands for *p*-JNK and JNK in VSMCs, with their respective quantifications. (J and K) Mitochondrial morphology in MitoTracker-stained VSMCs and quantification.

(L and M) Representative images of α-SMA immunofluorescence staining and quantification of average fluorescence intensity.

(N and O) Typical immunofluorescence images of *p*-JNK and quantification. Data are derived from three independent experiments, and all data are presented as mean ± S.E.M. *$p < 0.05$, **$p < 0.01$, ***$p < 0.001$, ****$p < 0.0001$. ns = no significant difference.

affecting the rate of lipid absorption and reducing the formation of postprandial chylomicrons.[40] Additionally, SA can reduce the accumulation of visceral fat,[41] which has been shown to be closely related to the development of hypertension and coronary artery disease.[42,43] Therefore, we hypothesized that SA may have an impact on AMD development. Indeed, consistent with our hypothesis, SA reduced the mortality and severity of AMD induced by BAPN in mice. However, Harvey KA et al. suggest that SA can promote apoptosis and inflammatory responses in human aortic endothelial cells (HAEC), [44] and endothelial damage is the initiation of atherosclerosis. This contradiction may be due to the different cells affected by SA. HAEC are located in the intima of the aorta, in direct contact with bloodstream, and are sensitive to changes in circulation.[45] In contrast, VSMCs are located in the media of the aorta, and the same stimuli may elicit different responses in them. Additionally, different signaling pathways may also play a role. For example, in cortical neurons, SA can counteract oxidative stress by activating PPARγ, providing neuroprotection.[11] In this study, SA regulates the phenotypic transformation of VSMCs and the homeostasis of mitochondrial dynamics by inhibiting the JNK/MAPK signaling, thus playing a protective role in AMD. The pathogenesis of AMD is complex, involving multiple cells and signaling pathways, and the effects of SA on different cells in AMD warrant further investigation.

Mitochondria are dynamic, semi-autonomous organelles, and mitochondrial processes including fusion, fission, selective degradation, and transport are collectively termed mitochondrial dynamics.[46] Mitochondrial fusion is mediated by MFN2, MFN1, and OPA1. MFN2 and MFN1, transmembrane proteins located on the mitochondrial outer membrane, mainly mediate docking and fusion of mitochondria.[23,47] The fusion of the mitochondrial inner membrane is mediated by OPA1 and cardiolipin, a characteristic component of the mitochondrial inner membrane.[48] During mitochondrial fission, DRP1 is a key GTPase.[23] After being recruited to the mitochondrial outer membrane by FIS1, Mff, MiD49, and MiD51, DRP1 forms oligomers, inducing membrane constriction and rupture.[49] In our study, DRP1 expression increased in aortic VSMCs during AMD, while the expression of MFN2, MFN1, and OPA1 decreased, suggesting excessive fission of mitochondria, consistent with previous findings in abdominal aortic aneurysms.[28] Notably, after administering SA, both western blotting and immunofluorescence results indicated upregulation of MFN2, MFN1, and OPA1 and downregulation of DRP1. However, there was no significant difference in FIS1 expression between groups. This seems to have had only minimal impact on mitochondrial morphology, since TEM and MitoTracker staining revealed that mitochondrial fission increased in VSMCs during AMD, and SA could reverse this excessive fission phenomenon. DRP1 is recruited by four proteins including FIS1, but cells lacking FIS1 show little or no mitochondrial fission defects, suggesting that changes in FIS1 expression may have little impact on mitochondrial fission.[50] Similar results were found by Senyilmaz et al. in *Drosophila* cells, where SA supplementation promoted mitochondrial fusion in Drosophila S2 cells, countering the mitochondrial dysfunction caused by the loss of Parkinson's disease genes such as *Pink* or *Parkin*.[9] However, studies of SA and VSMCs in AMD are lacking. Our study demonstrates that SA can reduce mitochondrial fission and increase fusion in VSMCs during AMD. Cooper et al. used specific inhibitors (Mdiv-1) or gene editing of *Drp1* to demonstrate that inhibiting excessive mitochondrial fission in VSMCs can alleviate the development of abdominal aortic aneurysms.[28] Zhong et al. also reported similar results in AD.[29] Therefore, we speculate that SA alleviates AMD potentially by promoting mitochondrial fusion and reducing fission in VSMCs. Additionally, SA also improved the abnormal ultrastructure of mitochondria in aortic VSMCs of AMD mice, such as reduced electron density, edema, and vacuolation, which may also be related to its impact on mitochondrial dynamics.

VSMCs are primarily located in the aortic media, where they are vital to regulating vascular tone and diameter, thus, managing blood pressure and blood flow distribution.[51] VSMCs are not terminally differentiated cells and exhibit high plasticity. In healthy aortas, VSMCs exhibit a contractile phenotype and switch to a synthetic phenotype under inflammatory and injury stimuli.[52] The switching of a large number of aortic VSMCs from contractile to synthetic phenotype is a key mechanism in the formation of AMD.[53] Sunaga et al.[54] found that the absence of *Elovl6*, the rate-limiting enzyme mediating the elongation of PA to SA, led to a decrease in the expression of the contractile marker SM22α in VSMCs. However, this only suggests that changes in lipid metabolism of VSMCs may regulate their phenotypic switching, such as through accumulation of PA or deficiency of SA and its metabolites such as oleic acid. Until now, no studies have explored the effects of SA on the phenotypic transformation of VSMCs. We found that SA upregulated the contractile markers α-SMA and SM22α in VSMCs, indicating that SA can increase contractile VSMCs. Additionally, mitochondrial morphology can affect the phenotypic switching of VSMCs: the inhibition of mitochondrial fission can reduce the proliferation and migration of VSMCs, which are characteristics of the synthetic phenotype,[55] while promoting mitochondrial fusion can reduce the dedifferentiation of VSMCs.[56] Mitochondrial fusion facilitates cooperation between healthy and damaged mitochondria, reducing damage to maintain cellular homeostasis.[57] Therefore, in our study, SA may increase the contractile phenotype of VSMCs by promoting mitochondrial fusion, thereby reducing the formation of AMD.

c-JUN N-terminal kinase (JNK) is a key molecule in the MAPK pathway and is associated with cell proliferation, differentiation, and apoptosis.[33,58,59] The activation of JNK may exacerbate the development of AMD by promoting apoptosis in VSMCs[60] and by increasing the expression of matrix metalloproteinases and inflammatory factors.[61,62] In fact, we found a significant increase in JNK activation in aortic

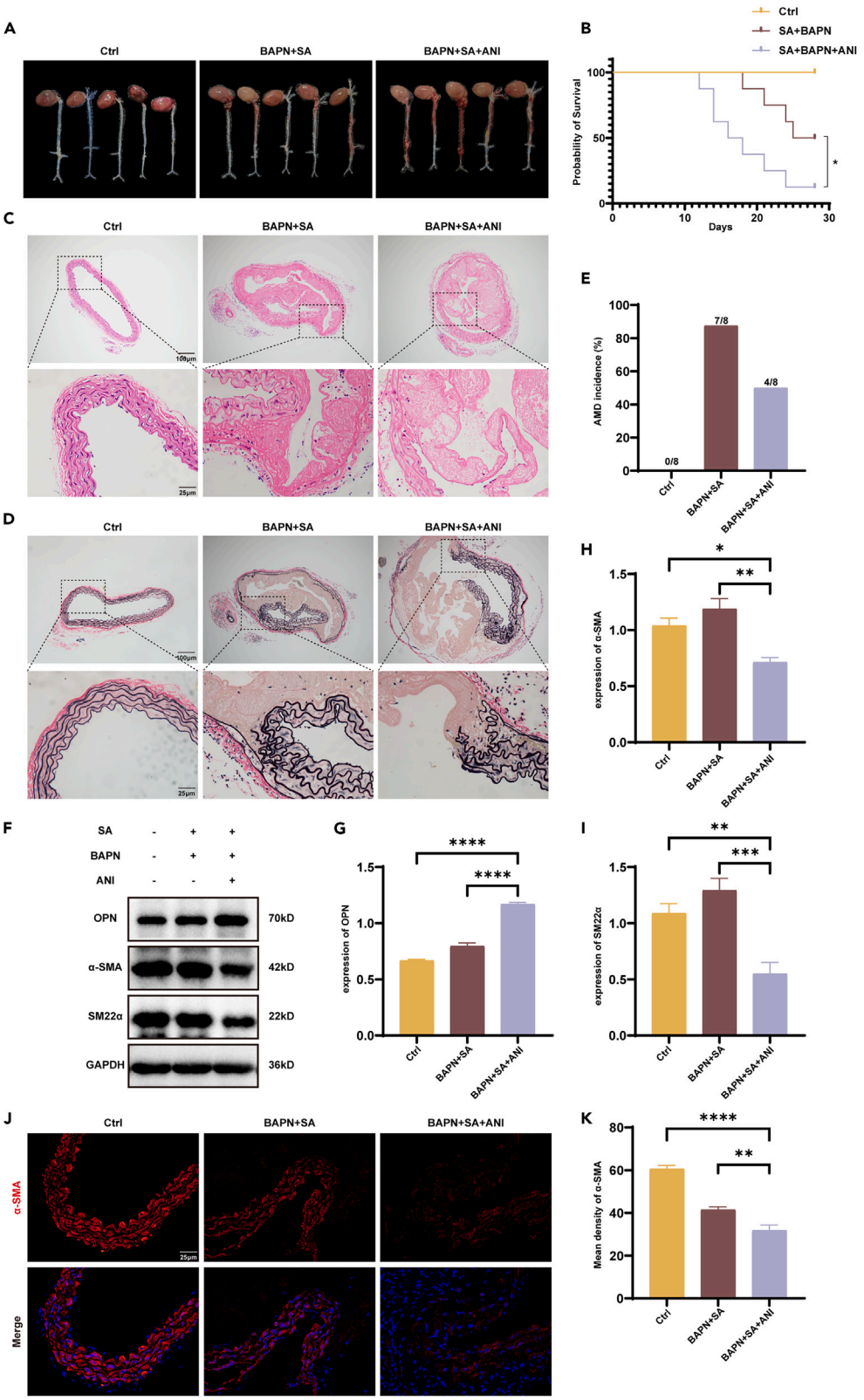
A
Ctrl
BAPN+SA
BAPN+SA+ANI
B
Ctrl
SA+BAPN
SA+BAPN+ANI
Probability of Survival
Days
C
D
E
AMD incidence (%)
7/8
4/8
0/8
F
SA
BAPN
ANI
OPN
α-SMA
SM22α
GAPDH
70kD
42kD
22kD
36kD
G
expression of OPN
H
expression of α-SMA
I
expression of SM22α
J
α-SMA
Merge
K
Mean density of α-SMA

**Figure 7. Activation of JNK abolishes the effect of SA in reducing BAPN-induced AMD formation in mice**

(A) Representative images of mouse aorta specimens.

(B) Survival curves of the three groups of mice.

(C and D) Representative images of H&E-stained (C) and EVG-stained (D) mouse aorta sections.

(E) AMD incidence of each group.

(F–I) Representative western blots of α-SMA, SM22α and OPN, along with statistical analyses of their expression levels.

(J and K) Immunofluorescence detection of the contractile phenotype marker α-SMA in aortic tissues of those three groups, along with quantification of their expression. Data are derived from three independent experiments, and all data are presented as mean ± S.E.M. *$p < 0.05$, **$p < 0.01$, ***$p < 0.001$, ****$p < 0.0001$.

specimens of AD patients, which was consistent with findings both *in vivo* and *in vitro*. SA markedly reduced JNK activation during AMD development. This is consistent with Senyilmaz et al.'s findings, which demonstrated that SA can inhibit JNK phosphorylation in HeLa cells.[9] Conversely, Spigoni et al.[63] suggested that SA can activate JNK in circulating angiogenic cells, inducing apoptosis. This discrepancy may be related to differences in the duration and concentration of SA exposure, as well as the cell types affected. Additionally, serum starvation prior to cell treatment can promote JNK phosphorylation,[64] potentially leading to false positive results. These reasons may explain the varied effects of SA on JNK. Furthermore, the introduction of ANI, a specific JNK activator, reversed the effect of SA in promoting mitochondrial fusion, increasing contractile phenotype, and reducing AMD formation in VSMCs. Thus, SA exerts its effects in AMD by inhibiting JNK/MAPK signaling.

In summary, our study proposes that SA, as a SFA, promotes mitochondrial fusion and increases contractile VSMCs by inhibiting JNK/MAPK signaling, thereby mitigating the progression of AMD for the first time. Based on our findings, altering the composition of fatty acids in daily diet may potentially serve as a method for preventing and treating AMD.

### Limitations of the study

This study has some limitations. Due to experimental constraints, we were unable to test the serum lipid composition of patients with AMD compared with healthy individuals. Additionally, there are several AMD animal models, and we only selected one, which may not comprehensively represent the condition. Finally, we did not utilize genetically edited animals to verify our hypothesis.

## STAR★METHODS

Detailed methods are provided in the online version of this paper and include the following:

- KEY RESOURCES TABLE
- RESOURCE AVAILABILITY
  - Lead contact
  - Materials availability
  - Data and code availability
- EXPERIMENTAL MODEL AND STUDY PARTICIPANT DETAILS
  - Human tissue samples
  - Animals and treatments
  - Cell culture and treatment
- METHOD DETAILS
  - Hematoxylin and eosin (H&E) staining
  - Elastic van gieson (EVG) staining
  - Immunofluorescence and immunohistochemistry
  - Western blotting
  - Transmission electron microscopy (TEM)
- QUANTIFICATION AND STATISTICAL ANALYSIS

## SUPPLEMENTAL INFORMATION

Supplemental information can be found online at https://doi.org/10.1016/j.isci.2024.110594.

## ACKNOWLEDGMENTS

This study was supported by the National Natural Science Foundation of China (No. 81700414 and No. 82070481).

## AUTHOR CONTRIBUTIONS

K.W. and X.X. contributed equally to this work. K.W.: Conceptualization, investigation, methodology, visualization and writing – original draft. X.X.: Conceptualization, investigation and methodology. X.H.: Conceptualization, supervision, funding acquisition and writing – reviewing and editing. Z.W.: Conceptualization and supervision. J.X.: Formal analysis and data curation. Q.W.: Methodology and data curation.

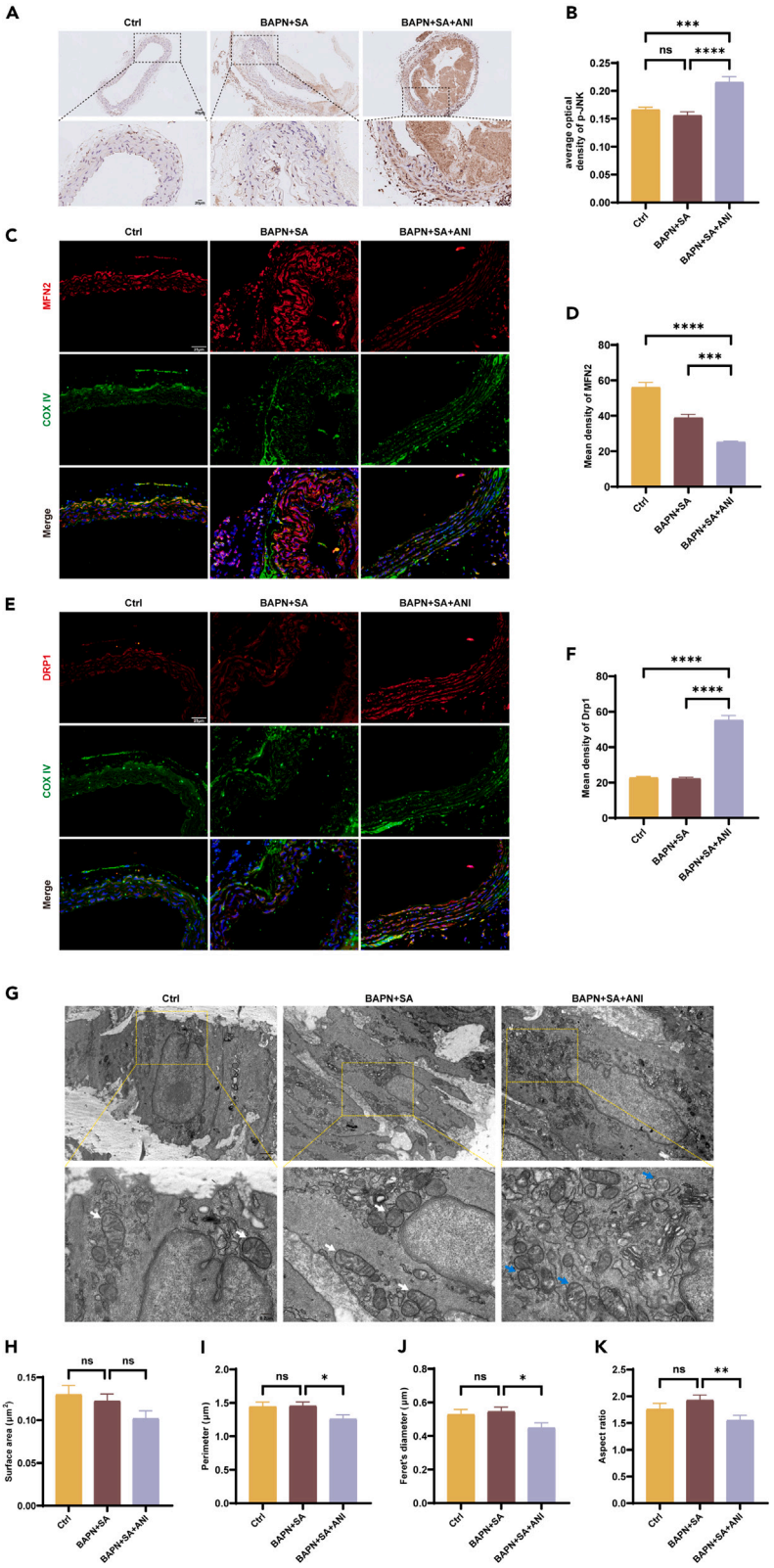
A
Ctrl
BAPN+SA
BAPN+SA+ANI
B
***
ns
****
average optical density of p-JNK
0.25
0.20
0.15
0.10
0.05
0.00
Ctrl
BAPN+SA
BAPN+SA+ANI
C
Ctrl
BAPN+SA
BAPN+SA+ANI
MFN2
COX IV
Merge
D
****
***
Mean density of MFN2
80
60
40
20
0
Ctrl
BAPN+SA
BAPN+SA+ANI
E
Ctrl
BAPN+SA
BAPN+SA+ANI
DRP1
COX IV
Merge
F
****
****
Mean density of Drp1
80
60
40
20
0
Ctrl
BAPN+SA
BAPN+SA+ANI
G
Ctrl
BAPN+SA
BAPN+SA+ANI
H
ns
ns
Surface area (μm²)
0.15
0.10
0.05
0.00
Ctrl
BAPN+SA
BAPN+SA+ANI
I
ns
*
Perimeter (μm)
2.0
1.5
1.0
0.5
0.0
Ctrl
BAPN+SA
BAPN+SA+ANI
J
ns
*
Feret's diameter (μm)
0.8
0.6
0.4
0.2
0.0
Ctrl
BAPN+SA
BAPN+SA+ANI
K
ns
**
Aspect ratio
2.5
2.0
1.5
1.0
0.5
0.0
Ctrl
BAPN+SA
BAPN+SA+ANI

**Figure 8. Activation of JNK negates the effect of SA on mitochondrial fusion in aortic VSMCs of AMD mice**

(A and B) Representative immunohistochemistry images of *p*-JNK in aortic sections from various mouse groups and quantification of *p*-JNK expression levels.

(C–F) Dual immunofluorescence staining results of MFN2 and COX IV, DRP1 and COX IV in aortic tissues of three mouse groups, along with corresponding quantifications.

(G) Transmission electron microscopy images of mitochondria in aortic VSMCs from different mouse groups. White arrows indicate normal mitochondria, while blue arrows represent mitochondria with abnormal structures.

(H–K) Analysis of mitochondrial morphological metrics including surface area, perimeter, Feret's diameter, and aspect ratio. >30 mitochondria were measured in each group. Data are derived from three independent experiments, and all data are presented as mean ± S.E.M. $*p < 0.05$, $**p < 0.01$, $***p < 0.001$, $****p < 0.0001$. ns = no significant difference.

## DECLARATION OF INTERESTS

The authors declare no competing interests.

Received: March 20, 2024
Revised: June 14, 2024
Accepted: July 24, 2024
Published: July 26, 2024

## REFERENCES

1. Daily, P.O., Trueblood, H.W., Stinson, E.B., Wuerflein, R.D., and Shumway, N.E. (1970). Management of acute aortic dissections. Ann. Thorac. Surg. *10*, 237–247. https://doi.org/10.1016/s0003-4975(10)65594-4.
2. Pape, L.A., Awais, M., Woznicki, E.M., Suzuki, T., Trimarchi, S., Evangelista, A., Myrmel, T., Larsen, M., Harris, K.M., Greason, K., et al. (2015). Presentation, Diagnosis, and Outcomes of Acute Aortic Dissection: 17-Year Trends From the International Registry of Acute Aortic Dissection. J. Am. Coll. Cardiol. *66*, 350–358. https://doi.org/10.1016/j.jacc.2015.05.029.
3. Trimarchi, S., Nienaber, C.A., Rampoldi, V., Myrmel, T., Suzuki, T., Mehta, R.H., Bossone, E., Cooper, J.V., Smith, D.E., Menicanti, L., et al. (2005). Contemporary results of surgery in acute type A aortic dissection: The International Registry of Acute Aortic Dissection experience. J. Thorac. Cardiovasc. Surg. *129*, 112–122. https://doi.org/10.1016/j.jtcvs.2004.09.005.
4. Nienaber, C.A., Clough, R.E., Sakalihasan, N., Suzuki, T., Gibbs, R., Mussa, F., Jenkins, M.P., Thompson, M.M., Evangelista, A., Yeh, J.S.M., et al. (2016). Aortic dissection. Nat. Rev. Dis. Prim. *2*, 1–18.
5. Mallat, Z., Tedgui, A., and Henrion, D. (2016). Role of Microvascular Tone and Extracellular Matrix Contraction in the Regulation of Interstitial Fluid: Implications for Aortic Dissection. Arterioscler. Thromb. Vasc. Biol. *36*, 1742–1747. https://doi.org/10.1161/ATVBAHA.116.307909.
6. Shen, Y.H., LeMaire, S.A., Webb, N.R., Cassis, L.A., Daugherty, A., and Lu, H.S. (2020). Aortic aneurysms and dissections series. Arterioscler. Thromb. Vasc. Biol. *40*, e37–e46.
7. Yang, K., Ren, J., Li, X., Wang, Z., Xue, L., Cui, S., Sang, W., Xu, T., Zhang, J., Yu, J., et al. (2020). Prevention of aortic dissection and aneurysm via an ALDH2-mediated switch in vascular smooth muscle cell phenotype. Eur. Heart J. *41*, 2442–2453. https://doi.org/10.1093/eurheartj/ehaa352.
8. Sampath, H., and Ntambi, J.M. (2005). The fate and intermediary metabolism of stearic acid. Lipids *40*, 1187–1191. https://doi.org/10.1007/s11745-005-1484-z.
9. Senyilmaz, D., Virtue, S., Xu, X., Tan, C.Y., Griffin, J.L., Miller, A.K., Vidal-Puig, A., and Teleman, A.A. (2015). Regulation of mitochondrial morphology and function by stearoylation of TFR1. Nature *525*, 124–128. https://doi.org/10.1038/nature14601.
10. Kim, H.S., Yoo, H.J., Lee, K.M., Song, H.E., Kim, S.J., Lee, J.O., Hwang, J.J., and Song, J.W. (2021). Stearic acid attenuates profibrotic signalling in idiopathic pulmonary fibrosis. Respirology *26*, 255–263. https://doi.org/10.1111/resp.13949.
11. Wang, Z.J., Liang, C.L., Li, G.M., Yu, C.Y., and Yin, M. (2007). Stearic acid protects primary cultured cortical neurons against oxidative stress. Acta Pharmacol. Sin. *28*, 315–326. https://doi.org/10.1111/j.1745-7254.2007.00512.x.
12. Bossone, E., LaBounty, T.M., and Eagle, K.A. (2018). Acute aortic syndromes: diagnosis and management, an update. Eur. Heart J. *39*, 739–749d. https://doi.org/10.1093/eurheartj/ehx319.
13. Grande, F., Anderson, J.T., and Keys, A. (1970). Comparison of effects of palmitic and stearic acids in the diet on serum cholesterol in man. Am. J. Clin. Nutr. *23*, 1184–1193. https://doi.org/10.1093/ajcn/23.9.1184.
14. Hunter, J.E., Zhang, J., and Kris-Etherton, P.M. (2010). Cardiovascular disease risk of dietary stearic acid compared with trans, other saturated, and unsaturated fatty acids: a systematic review. Am. J. Clin. Nutr. *91*, 46–63. https://doi.org/10.3945/ajcn.2009.27661.
15. Siri-Tarino, P.W., Sun, Q., Hu, F.B., and Krauss, R.M. (2010). Saturated fatty acids and risk of coronary heart disease: modulation by replacement nutrients. Curr. Atherosclerosis Rep. *12*, 384–390. https://doi.org/10.1007/s11883-010-0131-6.
16. Kris-Etherton, P.M., Griel, A.E., Psota, T.L., Gebauer, S.K., Zhang, J., and Etherton, T.D. (2005). Dietary stearic acid and risk of cardiovascular disease: intake, sources, digestion, and absorption. Lipids *40*, 1193–1200. https://doi.org/10.1007/s11745-005-1485-y.
17. Kuhn, T., Floegel, A., Sookthai, D., Johnson, T., Rolle-Kampczyk, U., Otto, W., von Bergen, M., Boeing, H., and Kaaks, R. (2016). Higher plasma levels of lysophosphatidylcholine 18:0 are related to a lower risk of common cancers in a prospective metabolomics study. BMC Med. *14*, 13. https://doi.org/10.1186/s12916-016-0552-3.
18. Senyilmaz-Tiebe, D., Pfaff, D.H., Virtue, S., Schwarz, K.V., Fleming, T., Altamura, S., Muckenthaler, M.U., Okun, J.G., Vidal-Puig, A., Nawroth, P., and Teleman, A.A. (2018). Dietary stearic acid regulates mitochondria in vivo in humans. Nat. Commun. *9*, 3129. https://doi.org/10.1038/s41467-018-05614-6.
19. Liesa, M., Palacín, M., and Zorzano, A. (2009). Mitochondrial dynamics in mammalian health and disease. Physiol. Rev. *89*, 799–845. https://doi.org/10.1152/physrev.00030.2008.
20. Frey, T.G., and Mannella, C.A. (2000). The internal structure of mitochondria. Trends Biochem. Sci. *25*, 319–324. https://doi.org/10.1016/s0968-0004(00)01609-1.
21. Zhu, T., Hu, Q., Yuan, Y., Yao, H., Zhang, J., and Qi, J. (2023). Mitochondrial dynamics in vascular remodeling and target-organ damage. Front. Cardiovasc. Med. *10*, 1067732. https://doi.org/10.3389/fcvm.2023.1067732.
22. Malka, F., Guillery, O., Cifuentes-Diaz, C., Guillou, E., Belenguer, P., Lombès, A., and Rojo, M. (2005). Separate fusion of outer and inner mitochondrial membranes. EMBO Rep. *6*, 853–859. https://doi.org/10.1038/sj.embor.7400488.
23. Adebayo, M., Singh, S., Singh, A.P., and Dasgupta, S. (2021). Mitochondrial fusion and fission: The fine-tune balance for cellular homeostasis. Faseb. J. *35*, e21620. https://doi.org/10.1096/fj.202100067R.
24. Huang, Q., Zhan, L., Cao, H., Li, J., Lyu, Y., Guo, X., Zhang, J., Ji, L., Ren, T., An, J., et al. (2016). Increased mitochondrial fission promotes autophagy and hepatocellular carcinoma cell survival through the ROS-modulated coordinated regulation of the NFKB and TP53 pathways. Autophagy *12*, 999–1014.
25. Kerr, J.S., Adriaanse, B.A., Greig, N.H., Mattson, M.P., Cader, M.Z., Bohr, V.A., and Fang, E.F. (2017). Mitophagy and Alzheimer's Disease: Cellular and Molecular Mechanisms. Trends Neurosci. *40*, 151–166. https://doi.org/10.1016/j.tins.2017.01.002.

26. Schultz, J., Waterstradt, R., Kantowski, T., Rickmann, A., Reinhardt, F., Sharoyko, V., Mulder, H., Tiedge, M., and Baltrusch, S. (2016). Precise expression of Fis1 is important for glucose responsiveness of beta cells. J. Endocrinol. *230*, 81–91.
27. Quiles, J.M., and Gustafsson, Å.B. (2022). The role of mitochondrial fission in cardiovascular health and disease. Nat. Rev. Cardiol. *19*, 723–736. https://doi.org/10.1038/s41569-022-00703-y.
28. Cooper, H.A., Cicalese, S., Preston, K.J., Kawai, T., Okuno, K., Choi, E.T., Kasahara, S., Uchida, H.A., Otaka, N., Scalia, R., et al. (2021). Targeting mitochondrial fission as a potential therapeutic for abdominal aortic aneurysm. Cardiovasc. Res. *117*, 971–982.
29. Zhong, X., Wu, Q., Wang, Z., Zhang, M., Zheng, S., Shi, F., Chen, Y., Che, Y., Yuan, S., and Xing, K. (2022). Iron deficiency exacerbates aortic medial degeneration by inducing excessive mitochondrial fission. Food Funct. *13*, 7666–7683. https://doi.org/10.1039/d2fo01084d.
30. Li, B., Wang, Z., Hong, J., Che, Y., Chen, R., Hu, Z., Hu, X., Wu, Q., Hu, J., and Zhang, M. (2021). Iron deficiency promotes aortic medial degeneration via destructing cytoskeleton of vascular smooth muscle cells. Clin. Transl. Med. *11*, e276. https://doi.org/10.1002/ctm2.276.
31. Zhang, J., He, Z., Fedorova, J., Logan, C., Bates, L., Davitt, K., Le, V., Murphy, J., Li, M., Wang, M., et al. (2021). Alterations in mitochondrial dynamics with age-related Sirtuin1/Sirtuin3 deficiency impair cardiomyocyte contractility. Aging Cell *20*, e13419. https://doi.org/10.1111/acel.13419.
32. Ailawadi, G., Moehle, C.W., Pei, H., Walton, S.P., Yang, Z., Kron, I.L., Lau, C.L., and Owens, G.K. (2009). Smooth muscle phenotypic modulation is an early event in aortic aneurysms. J. Thorac. Cardiovasc. Surg. *138*, 1392–1399.
33. Hepp Rehfeldt, S.C., Majolo, F., Goettert, M.I., and Laufer, S. (2020). c-Jun N-terminal kinase inhibitors as potential leads for new therapeutics for Alzheimer's diseases. Int. J. Mol. Sci. *21*, 9677.
34. Shi, F., Wang, Z., Wu, Q., Zhong, X., Zhang, M., Li, B., Ren, W., Yuan, S., and Chen, Y. (2022). Iron deficiency promotes aortic media degeneration by activating endoplasmic reticulum stress-mediated IRE1 signaling pathway. Pharmacol. Res. *183*, 106366. https://doi.org/10.1016/j.phrs.2022.106366.
35. Xiang, Y., Zhou, Z., Zhu, L., Li, C., Luo, Y., and Zhou, J. (2023). Omentin-1 enhances the inhibitory effect of endothelial progenitor cells on neointimal hyperplasia by inhibiting the p38 MAPK/CREB pathway. Life Sci. *331*, 122061. https://doi.org/10.1016/j.lfs.2023.122061.
36. Wu, J., Zafar, M., Qiu, J., Huang, Y., Chen, Y., Yu, C., and Elefteriades, J.A. (2019). A systematic review and meta-analysis of isolated abdominal aortic dissection. J. Vasc. Surg. *70*, 2046–2053.e6. https://doi.org/10.1016/j.jvs.2019.04.467.
37. Zhao, L., Jin, H., Yang, B., Zhang, S., Han, S., Yin, F., and Feng, Y. (2016). Correlation between ABCA1 gene polymorphism and aopA-I and HDL-C in abdominal aortic aneurysm. Med. Sci. Mon. Int. Med. J. Exp. Clin. Res. *22*, 172–176.
38. Bonanome, A., and Grundy, S.M. (1988). Effect of dietary stearic acid on plasma cholesterol and lipoprotein levels. N. Engl. J. Med. *318*, 1244–1248. https://doi.org/10.1056/NEJM198805123181905.
39. van Rooijen, M.A., Plat, J., Blom, W.A.M., Zock, P.L., and Mensink, R.P. (2021). Dietary stearic acid and palmitic acid do not differently affect ABCA1-mediated cholesterol efflux capacity in healthy men and postmenopausal women: A randomized controlled trial. Clin. Nutr. *40*, 804–811.
40. Berry, S.E.E., Miller, G.J., and Sanders, T.A.B. (2007). The solid fat content of stearic acid–rich fats determines their postprandial effects. Am. J. Clin. Nutr. *85*, 1486–1494.
41. Shen, M.C., Zhao, X., Siegal, G.P., Desmond, R., and Hardy, R.W. (2014). Dietary stearic acid leads to a reduction of visceral adipose tissue in athymic nude mice. PLoS One *9*, e104083. https://doi.org/10.1371/journal.pone.0104083.
42. Hayashi, T., Boyko, E.J., Leonetti, D.L., McNeely, M.J., Newell-Morris, L., Kahn, S.E., and Fujimoto, W.Y. (2003). Visceral adiposity and the prevalence of hypertension in Japanese Americans. Circulation *108*, 1718–1723. https://doi.org/10.1161/01.CIR.0000087597.59169.8D.
43. Hiuge-Shimizu, A., Kishida, K., Funahashi, T., Okutsu, M., Kametani, R., Kobayashi, H., Nozaki, Y., Nomura, A., Yokoi, H., Yoshizumi, T., et al. (2012). Coexistence of visceral fat and multiple risk factor accumulations is strongly associated with coronary artery disease in Japanese (the VACATION-J study). J. Atherosclerosis Thromb. *19*, 657–663.
44. Harvey, K.A., Walker, C.L., Xu, Z., Whitley, P., Pavlina, T.M., Hise, M., Zaloga, G.P., and Siddiqui, R.A. (2010). Oleic acid inhibits stearic acid-induced inhibition of cell growth and pro-inflammatory responses in human aortic endothelial cells. J. Lipid Res. *51*, 3470–3480. https://doi.org/10.1194/jlr.M010371.
45. Wu, X., Zhang, H., Qi, W., Zhang, Y., Li, J., Li, Z., Lin, Y., Bai, X., Liu, X., Chen, X., et al. (2018). Nicotine promotes atherosclerosis via ROS-NLRP3-mediated endothelial cell pyroptosis. Cell Death Dis. *9*, 171. https://doi.org/10.1038/s41419-017-0257-3.
46. Chan, D.C. (2020). Mitochondrial Dynamics and Its Involvement in Disease. Annu. Rev. Pathol. *15*, 235–259. https://doi.org/10.1146/annurev-pathmechdis-012419-032711.
47. Mattie, S., Riemer, J., Wideman, J.G., and McBride, H.M. (2018). A new mitofusin topology places the redox-regulated C terminus in the mitochondrial intermembrane space. J. Cell Biol. *217*, 507–515. https://doi.org/10.1083/jcb.201611194.
48. Tilokani, L., Nagashima, S., Paupe, V., and Prudent, J. (2018). Mitochondrial dynamics: overview of molecular mechanisms. Essays Biochem. *62*, 341–360. https://doi.org/10.1042/EBC20170104.
49. Pagliuso, A., Cossart, P., and Stavru, F. (2018). The ever-growing complexity of the mitochondrial fission machinery. Cell. Mol. Life Sci. *75*, 355–374. https://doi.org/10.1007/s00018-017-2603-0.
50. Murata, D., Arai, K., Iijima, M., and Sesaki, H. (2020). Mitochondrial division, fusion and degradation. J. Biochem. *167*, 233–241. https://doi.org/10.1093/jb/mvz106.
51. Petsophonsakul, P., Furmanik, M., Forsythe, R., Dweck, M., Schurink, G.W., Natour, E., Reutelingsperger, C., Jacobs, M., Mees, B., and Schurgers, L. (2019). Role of vascular smooth muscle cell phenotypic switching and calcification in aortic aneurysm formation: Involvement of vitamin K-dependent processes. Arterioscler. Thromb. Vasc. Biol. *39*, 1351–1368.
52. Owens, G.K. (1995). Regulation of differentiation of vascular smooth muscle cells. Physiol. Rev. *75*, 487–517. https://doi.org/10.1152/physrev.1995.75.3.487.
53. Liu, R., Lo, L., Lay, A.J., Zhao, Y., Ting, K.K., Robertson, E.N., Sherrah, A.G., Jarrah, S., Li, H., Zhou, Z., et al. (2017). ARHGAP18 Protects Against Thoracic Aortic Aneurysm Formation by Mitigating the Synthetic and Proinflammatory Smooth Muscle Cell Phenotype. Circ. Res. *121*, 512–524. https://doi.org/10.1161/CIRCRESAHA.117.310692.
54. Sunaga, H., Matsui, H., Anjo, S., Syamsunarno, M.R.A.A., Koitabashi, N., Iso, T., Matsuzaka, T., Shimano, H., Yokoyama, T., and Kurabayashi, M. (2016). Elongation of Long-Chain Fatty Acid Family Member 6 (Elovl6)-Driven Fatty Acid Metabolism Regulates Vascular Smooth Muscle Cell Phenotype Through AMP-Activated Protein Kinase/Krüppel-Like Factor 4 (AMPK/KLF 4) Signaling. J. Am. Heart Assoc. *5*, e004014.
55. Salabei, J.K., and Hill, B.G. (2013). Mitochondrial fission induced by platelet-derived growth factor regulates vascular smooth muscle cell bioenergetics and cell proliferation. Redox Biol. *1*, 542–551. https://doi.org/10.1016/j.redox.2013.10.011.
56. Torres, G., Morales, P.E., García-Miguel, M., Norambuena-Soto, I., Cartes-Saavedra, B., Vidal-Peña, G., Moncada-Ruff, D., Sanhueza-Olivares, F., San Martín, A., and Chiong, M. (2016). Glucagon-like peptide-1 inhibits vascular smooth muscle cell dedifferentiation through mitochondrial dynamics regulation. Biochem. Pharmacol. *104*, 52–61.
57. Youle, R.J., and van der Bliek, A.M. (2012). Mitochondrial fission, fusion, and stress. Science *337*, 1062–1065. https://doi.org/10.1126/science.1219855.
58. Galeotti, N., and Ghelardini, C. (2012). Regionally selective activation and differential regulation of ERK, JNK and p38 MAP kinase signalling pathway by protein kinase C in mood modulation. Int. J. Neuropsychopharmacol. *15*, 781–793. https://doi.org/10.1017/S1461145711000897.
59. Tournier, C., Hess, P., Yang, D.D., Xu, J., Turner, T.K., Nimnual, A., Bar-Sagi, D., Jones, S.N., Flavell, R.A., and Davis, R.J. (2000). Requirement of JNK for stress-induced activation of the cytochrome c-mediated death pathway. Science *288*, 870–874. https://doi.org/10.1126/science.288.5467.870.
60. Ito, S., Ozawa, K., Zhao, J., Kyotani, Y., Nagayama, K., and Yoshizumi, M. (2015). Olmesartan inhibits cultured rat aortic smooth muscle cell death induced by cyclic mechanical stretch through the inhibition of the c-Jun N-terminal kinase and p38 signaling pathways. J. Pharmacol. Sci. *127*, 69–74.
61. Hu, Y., Lu, L., Qiu, Z., Huang, Q., Chen, Y., and Chen, L. (2018). Mechanical stretch aggravates aortic dissection by regulating MAPK pathway and the expression of MMP-9 and inflammation factors. Biomed. Pharmacother. *108*, 1294–1302. https://doi.org/10.1016/j.biopha.2018.09.129.

62. Karasaki, K., Kokubo, H., Bumdelger, B., Kaji, N., Sakai, C., Ishida, M., and Yoshizumi, M. (2023). Angiotensin II Type 1 Receptor Blocker Prevents Abdominal Aortic Aneurysm Progression in Osteoprotegerin-Deficient Mice via Upregulation of Angiotensin (1-7). J. Am. Heart Assoc. *12*, e027589. https://doi.org/10.1161/JAHA.122.027589.

63. Spigoni, V., Fantuzzi, F., Fontana, A., Cito, M., Derlindati, E., Zavaroni, I., Cnop, M., Bonadonna, R.C., and Dei Cas, A. (2017). Stearic acid at physiologic concentrations induces in vitro lipotoxicity in circulating angiogenic cells. Atherosclerosis *265*, 162–171.

64. Ji, K.Y., Kim, K.M., Kim, Y.H., Shim, K.S., Lee, J.Y., Kim, T., and Chae, S. (2021). Serum Starvation Sensitizes Anticancer Effect of Anemarrhena asphodeloides via p38/JNK-Induced Cell Cycle Arrest and Apoptosis in Colorectal Cancer Cells. Am. J. Chin. Med. *49*, 1001–1016. https://doi.org/10.1142/S0192415X21500488.

65. Zheng, H.Q., Rong, J.B., Ye, F.M., Xu, Y.C., Lu, H.S., and Wang, J.A. (2020). Induction of thoracic aortic dissection: a mini-review of beta-aminopropionitrile-related mouse models. J. Zhejiang Univ. - Sci. B *21*, 603–610. https://doi.org/10.1631/jzus.B2000022.

## STAR★METHODS

### KEY RESOURCES TABLE

| REAGENT or RESOURCE | SOURCE | IDENTIFIER |
|---|---|---|
| Antibodies | | |
| Anti-MFN2 antibody | Abcam | Cat#ab205236 |
| Anti-MFN1 antibody | Abcam | Cat#ab221661 |
| Anti-DRP1 antibody | Abcam | Cat#ab184247 |
| Anti-OPA1 antibody | Proteintech | Cat#27733-1-AP |
| Anti-Fis1 antibody | Proteintech | Cat#66635-1-Ig |
| Anti-α-SMA antibody | Servicebio | Cat#GB111364-100 |
| Anti-SM22α antibody | Servicebio | Cat#GB11366-100 |
| Anti-OPN antibody | Servicebio | Cat#GB112328-100 |
| Anti-JNK antibody | Proteintech | Cat#66210-1-Ig |
| Anti-Phospho-JNK antibody | Proteintech | Cat#80024-1-RR |
| Anti-Cox IV antibody | Proteintech | Cat#66110-1-Ig |
| Anti-GAPDH antibody | Servicebio | Cat#GB15004-100 |
| Anti-β-actin antibody | Servicebio | Cat#GB11001-100 |
| Anti-Rabbit IgG HRP conjugated antibody | Servicebio | Cat#GB23303 |
| Anti-Mouse IgG HRP conjugated antibody | Servicebio | Cat#GB23301 |
| Anti-Rabbit IgG Cy3 conjugated antibody | Servicebio | Cat#GB21303 |
| Anti-Mouse IgG FITC conjugated antibody | Servicebio | Cat#GB22301 |
| Chemicals, peptides, and recombinant proteins | | |
| Stearic acid | Sigma-Aldrich | Cat#175366 |
| Sodium stearate | Sigma-Aldrich | Cat#S3381-1G |
| β-aminopropionitrile | Yuanye | Cat#S44439-5g |
| Anisomycin | MedChemExpress | Cat#HY-18982 |
| Angiotensin II | MedChemExpress | Cat#HY-13948 |
| Bovine Serum Albumin | Beyotime | Cat#ST2254-5g |
| DMEM/F12 | HyClone | Cat#SH30023.01 |
| Fetal bovine serum | Gibco | Cat#A3160901 |
| Critical commercial assays | | |
| Mito-Tracker Red CMXRos | Beyotime | Cat#C1035-50μg |
| Experimental models: Organisms/strains | | |
| C57BL/6J | Shulaibao (Wuhan) Biotechnology | N/A |
| Software and algorithms | | |
| GraphPad Prism version 9.0.0 | GraphPad Software | https://www.graphpad.com/features |
| FIJI/ImageJ | NIH | https://hpc.nih.gov/apps/Fiji.html |

### RESOURCE AVAILABILITY

#### Lead contact

Further information about the protocols and requests for resources and reagents should be directed to and will be fulfilled by the lead contact, Xiaoping Hu xiaoping8205@whu.edu.cn.

#### Materials availability

This study did not generate new unique reagents.

### Data and code availability

- All data reported in this paper will be shared by the lead contact upon request.
- No new code was generated in this study.
- Any additional information required to reanalyze the data reported in this paper is available from the lead contact upon request.

## EXPERIMENTAL MODEL AND STUDY PARTICIPANT DETAILS

### Human tissue samples

The Clinical Research Ethics Committee of Renmin Hospital of Wuhan University approved the study protocol (WDRY2020-K230), and the study adheres to the Declaration of Helsinki and its amendments. Specimens were collected between January 2021 and December 2023. All patients and donors signed written informed consent forms. Aortic specimens of AMD were obtained from AD patients undergoing surgical treatment ($n = 6$). Normal aortic specimens were obtained from organ donors without aortic lesions ($n = 6$). All specimens were preserved in liquid nitrogen or 4% formaldehyde after removal of the intima and adventitia. The gender, age, and ethnicity information of all participants can be seen in Table S1.

### Animals and treatments

All animal experiments were performed with approval of the Ethics Committee of the Renmin Hospital of Wuhan University (WDRM-20201107). And protocols were in compliance with the Wuhan Directive for Animal Research and the Current Guidelines for the NIH Care and Use of Laboratory Animals. β-aminopropionitrile (BAPN) was used to establish AD in mice as previously reported.[65] Stearic acid concentrations were determined as previously.[41] Anisomycin (ANI), a JNK activator, specifically increases expression of phosphorylated JNK. First, 60 three-week-old C57BL/6J male mice were randomly divided into four groups ($n = 15$ per group): Ctrl (regular diet), SA (17% SA diet), BAPN (0.25% BAPN diet), and BAPN+SA (17% SA+0.25% BAPN diet). In subsequent animal experiments, 24 three-week-old male C57BL/6J mice were randomly divided into three groups ($n = 8$ per group): Ctrl (regular diet), BAPN+SA (17% SA + 0.25% BAPN diet), and BAPN+SA+ANI (17% SA + 0.25% BAPN diet and ANI 10 mg/kg d i.p.). In the relevant groups, mice were fed a 17% SA diet for five days in advance. Then, the AD model was established with BAPN. Mice were monitored daily. Survival and causes of death were recorded. When deceased mice were discovered, their aortas were immediately harvested to ensure the specimens were fresh. Mice that did not die were euthanized with 1% phenobarbital and aortas were harvested and fixed with 4% formaldehyde over 24 h after 28 days.

### Cell culture and treatment

As described in previous literature,[29] primary vascular smooth muscle cells (VSMCs) were isolated from 6-week-old male Sprague-Dawley rats and cultured in DMEM/F12 medium containing 10% fetal bovine serum and 1% penicillin/streptomycin under 5% $CO_2$ at 37°C. Angiotensin II (AngII) was used to mimic the pathological changes of AD. Sodium SA (5 mM) was added to prepared 2 mM fatty acid-free and low-endotoxin BSA in PBS and then sonicated until dissolved. Initially, VSMCs were divided into four groups: Ctrl, SA, AngII, and AngII+SA. In later experiments, another four groups were Ctrl, AngII, AngII+SA, AngII+SA+ANI. MitoTracker was used to stain mitochondria. A certain concentration of working solution was incubated with VSMCs at 37°C for 30 min. Observation was performed by confocal microscopy.

## METHOD DETAILS

### Hematoxylin and eosin (H&E) staining

All fresh aortic specimens were fixed in 4% paraformaldehyde for over 24 h. Then, targeted sections of the aorta were excised, dehydrated, infiltrated by paraffin and sectioned.

Paraffin sections, after undergoing a series of xylene and alcohol treatments for deparaffinization and hydration, were stained with hematoxylin. Excess hematoxylin was rinsed off. Subsequently, sections were stained with eosin. Sections were then dehydrated using an alcohol gradient and immersed in xylene twice, each for 5 min. Finally, sections were sealed with neutral gum.

### Elastic van gieson (EVG) staining

After deparaffinization and hydration, sections were immersed in Verhoeff's hematoxylin solution, followed by rinsing. Iron trichloride differentiation liquid was then applied to differentiate the elastic fibers until they appeared black against a gray background. Next, Van Gieson's solution was used to stain sections, and sections were rinsed and dehydrated with absolute ethanol. Eventually, sections were immersed in xylene and mounted.

### Immunofluorescence and immunohistochemistry

After deparaffinization and hydration, sections were treated with 0.2% Triton. Sections were immersed in sodium citrate solution and heated in a microwave for antigen retrieval. Additionally, sections of VSMCs were fixed with 4% formaldehyde and immersed in 0.2% Triton. Sections were blocked with 3% BSA for 40 min.

For immunofluorescence, the primary antibodies, anti-MFN2, anti-OPA1, anti-DRP1, anti-α-SMA, anti-COX IV and anti-phospho-JNK, were prepared at specific dilutions and incubated with sections at 4°C overnight. Then, sections were incubated at room temperature in

the dark with the Cy3-conjugated or FITC-conjugated secondary antibody for 1 h. Finally, sections were incubated with DAPI, then washed and mounted. Tissue sections were observed and images captured by fluorescence microscopy.

For immunohistochemistry, following antigen retrieval, sections were immersed into 3% $H_2O_2$ in the dark. Subsequently, sections were blocked and incubated with primary antibodies, anti-phospho-JNK. This was followed by incubation with HRP-conjugated secondary antibody, after which sections were washed and stained with DAB for a uniform staining time. Finally, cell nuclei were counterstained with hematoxylin before being mounted in glass slides.

### Western blotting

Aortic tissue and VSMCs were lysed on ice by protein lysis buffer containing RIPA, cocktail, PMSF, and phosphatase inhibitor in a specific ratio to extract the proteins. The extracted proteins were separated through SDS-PAGE gels (10–12%) and transferred onto a transfer membrane. Protein membranes were blocked with Rapid Blocking Buffer. After that, the membrane was incubated with primary antibodies: anti-MFN2, anti-MFN1, anti-OPA1, anti-Drp1, anti Fis1, anti-OPN, anti-α-SMA, anti-SM22α, anti-phospho-JNK, anti-JNK, anti-GAPDH, and anti-β-actin at 4°C for over 12 h. Then, membranes were washed and incubated with secondary antibodies. Finally, the membrane was washed and immersed in enhanced chemiluminescent reagent and imaged with a chemiluminescent imaging system.

### Transmission electron microscopy (TEM)

Mice were euthanized with 1% pentobarbital solution. The target region of the aorta was rapidly dissected and immersed in pre-chilled EM fixative. Tissues were fixed at room temperature for 1 h, then fixed at 4°C overnight. The fixed samples were then sent to Servicebio Co., Ltd. for further processing.

## QUANTIFICATION AND STATISTICAL ANALYSIS

Statistical analyses were performed using GraphPad Prism v9.0.0 (GraphPad Software, USA). As for quantitative data which pass tests for normality or homogeneity of variance, Student's t test was used to compare two groups, while one-way ANOVA was used for multiple group comparisons. In cases where quantitative data did not pass tests for normality or homogeneity of variance, the Mann–Whitney test was used to compare two groups and the Kruskal-Wallis for more than two groups. The $\chi^2$ test was used for categorical data. A significance level of $p < 0.05$ indicated statistical significance.